Clays and Clay Minerals, Vol. 48, No. 5, 521–527, 2000.

STRUCTURAL CHEMISTRY OF Fe, Mn, AND Ni IN SYNTHETIC HEMATITES AS DETERMINED BY EXTENDED X-RAY ABSORPTION FINE STRUCTURE SPECTROSCOPY

BALWANT SINGH,[1] D.M. SHERMAN,[2] R.J. GILKES,[3] M. WELLS,[4] AND J.F.W. MOSSELMANS[5]

[1] Department of Agricultural Chemistry & Soil Science, The University of Sydney, Sydney, Australia
[2] Department of Geology, University of Bristol, Bristol, UK
[3] Department of Soil Science & Plant Nutrition, University of Western Australia, Nedlands, Australia
[4] CRC LEME, University of Canberra, Belconnen, A.C.T., Australia
[5] CCLRC, Daresbury Laboratory, Warrington, UK

Abstract—The incorporation of transition metals into hematite may limit the aqueous concentration and bioavailabity of several important nutrients and toxic heavy metals. Before predicting how hematite controls metal-cation solubility, we must understand the mechanisms by which metal cations are incorporated into hematite. Thus, we have studied the mechanism for Ni^{2+} and Mn^{3+} uptake into hematite using extended X-ray absorption fine structures (EXAFS) spectroscopy. EXAFS measurements show that the coordination environment of Ni^{2+} in hematite corresponds to that resulting from Ni^{2+} replacing Fe^{3+}. No evidence for NiO or $Ni(OH)_2$ was found. The infrared spectrum of Ni-substituted hematite shows an OH-stretch band at 3168 cm^{-1} and Fe-OH bending modes at 892 and 796 cm^{-1}. These vibrational bands are similar to those found in goethite. The results suggest that the substitution of Ni^{2+} for Fe^{3+} is coupled with the protonation of one of the hematite oxygen atoms to maintain charge balance.

The solubility of Mn^{3+} in hematite is much less extensive than that of Ni^{2+} because of the strong Jahn-Teller distortion of Mn^{3+} in six-fold coordination. Structural evidence of Mn^{3+} substituting for Fe^{3+} in hematite was found for a composition of 3.3 mole % Mn_2O_3. However a sample with nominally 6.6 mole % Mn_2O_3 was found to consist of two phases: hematite and ramsdellite (MnO_2). The results indicate that for cations, such as Mn^{3+} showing a strong Jahn-Teller effect, there is limited substitution in hematite.

Key Words—EXAFS, Fe Oxides, Hematite, Metal Substitution, Trace Elements, XAS, XRD.

INTRODUCTION

Hematite is a common mineral in many tropical and sub-tropical soils, and it usually occurs in association with goethite (Schwertmann and Taylor, 1989). The prevalence of Al in weathering environments results in the substitution of Al^{3-} for Fe^{3+} in hematite (α-Fe_2O_3), and this substitution is well documented both for natural and synthetic hematite (Schwertmann *et al.*, 1979; Bigham *et al.*, 1978; Kosmas *et al.*, 1986; Singh and Gilkes, 1992). Samples with ≤16 mole % Al substitution have been reported in synthetic and natural hematites (Schwertmann *et al.*, 1979; Singh and Gilkes, 1992). Aluminum substitution in hematite is usually determined from the shift in X-ray diffraction (XRD) lines owing to the presence of slightly smaller Al^{3+} ions (0.53 Å) replacing Fe^{3+} ions (0.65 Å), thereby contracting the unit-cell dimensions.

Similar substitutions of other cations, such as Mn^{3+}, Ni^{2+}, Cr^{3+}, and Ti^{4+} are possible in the structure of hematite, hematite substituted with these cations has been synthesized (Sidhu *et al.*, 1980; Vandenberghe *et al.*, 1986; Cornell *et al.*, 1992). There are few reports indicating the substitution of trace elements in natural hematite (Singh and Gilkes, 1992). The level of substitution of these elements is generally much smaller compared to Al, and as the size of some substituting cations is quite similar to Fe^{3-} (Shannon and Prewitt, 1969), there is a little or no observable shift in XRD lines. Thus, XRD can not be used to determine these substitutions. The degree of congruency during dissolution has been used to verify the structural incorporation of foreign cations in the structure of hematite, but this technique is not truly specific (Singh and Gilkes, 1991; Trolard *et al.*, 1995). Various spectral techniques [*e.g.*, Mössbauer, Infrared (IR), and Visible-light spectroscopy] have also been investigated, but none has been shown to be both highly specific and sensitive to minor amount of substitution.

In recent years, extended X-ray absorption fine structure (EXAFS) spectroscopy has been successfully used to refine the structure of many oxide minerals, including Fe oxides (Manceau and Combes, 1988; Combes *et al.*, 1990). The technique is capable of providing information about the local structure, such as nearest neighbors and coordination numbers, around the X-ray absorbing atom. In this study we used synchrotron-based EXAFS spectroscopy to determine the local structure around Fe, Mn, and Ni ions in some well-characterized synthetic hematite samples.

MATERIALS AND METHODS

For the synthesis of metal-substituted hematites, the appropriate quantity of the metal (Al^{3+}, Mn^{2+}, and Ni^{2+}) nitrate salt was added to 1 M ferric nitrate solution and mixed thoroughly. Approximately 4 M

Table 1. Crystallographic properties derived from XRD analysis and N_2-BET surface areas (S.A.) of hematite samples (see text for other abbreviations).

Sample detail	*a* [1](nm)	*c* [1](nm)	Volume (nm^3)	MCD_a (nm)	MCD_c (nm)	S.A. (m^2/g)
Natural hematite (France)	0.5032 (5)	1.3735 (8)	0.3012	nd	nd	0.4
Hematite 4.6 mole % Al	0.5023 (5)	1.3732 (7)	0.3001	31.3	38.9	15.9
Hematite 15 mole % Al	0.5008 (6)	1.3692 (15)	0.2974	18.7	5.2	46.5
Hematite 3.3 mole % Mn	0.5033 (5)	1.3751 (7)	0.3017	nd	38.6	16.3
Hematite 6.3 mole % Mn	0.5036 (6)	1.3746 (10)	0.3019	26.0	23.1	13.8
Hematite 1.1 mole % Ni	0.5031 (5)	1.3757 (8)	0.3016	44.3	29.4	16.6
Hematite 6.0 mole % Ni	0.5040 (5)	1.3783 (8)	0.3032	49.5	49.3	12.6

[1] Values in parentheses are the estimated standard deviation for the last digit for the two cell parameters.

NH_4OH solution was added with vigorous stirring using a magnetic stirrer and plastic rod until NH_4^+ was in 30% excess of the stoichiometric quantity to precipitate Fe and the associated metal cation as a mixed Fe-Me-hydroxide gel (Fisher and Schwertmann, 1975).

The gel was collected by centrifugation and washed using three lots of 200 mL of deionized water. After washing, the precipitated gel was transferred to 1000 mL Pyrex-stoppered reagent bottles and resuspended with 900 mL deionized water to give a suspension concentration of 12.4 g Fe L^{-1}, and pH was adjusted between 7.5–8.0. Suspensions were then placed in an oven at 90°C and aged for 14 d. During aging, the suspension was mixed regularly by repeated inversion and pH was maintained between 7.5–8.0, using either 0.5 M HCl or 0.2 M KOH solution. At the end of the equilibration period, suspensions were centrifuged, solids washed three times with deionized water followed by a single wash in 50 mL acetone before drying overnight at 50°C. Samples were then gently crushed using an agate mortar and pestle and stored in a dessicator prior to analysis.

Ammonium-oxalate treatment was used to remove amorphous Fe oxides and any metals/cations that may be associated with them. The treatment consisted of two consecutive 60-min washes with 0.2 M ammonium oxalate (pH = 3) at 20°C in the dark (McKeague and Day, 1966), using a sample : solution ratio of 1: 200 (Parfitt, 1989). The substitution of various elements in the structure of hematite was calculated from the chemical analysis of ammonium-oxalate pretreated samples. All other analyses, including EXAFS spectroscopy, were also done on oxalate pretreated samples.

The surface area of hematite samples was determined by the multipoint N_2-BET method using a computer-controlled Micromeritics Gemini 2375 instrument after degassing the samples overnight at 100°C.

XRD analysis was performed using CuKα radiation with a computer-controlled Philips PW 1050 vertical goniometer with 1° receiving and divergence slits, and a graphite diffracted-beam monchromator. For accurate measurements of *d* values, XRD patterns were obtained using a scan speed of 0.3 °2θ min^{-1} and a step size of 0.01 °2θ with 10% NaCl added as an internal standard to correct for line broadening and instrumental shifts in *d* value. The unit-cell dimensions of hematite were calculated from the 012, 104, 110, 113, 116, 018, 214, and 300 reflections, using a crystallographic *least-squares* refinement program (Novak and Colville, 1989). Mean crystallite dimensions (MCD) along the hematite *a* and *c* crystallographic axes were determined using the Scherrer equation (Klug and Alexander, 1974).

For IR spectroscopy, 13-mm diameter pressed discs (1 mg sample + 170 mg KBr) were used and spectra were recorded on a Nicolet Magna-IR 550 Fourier-transform infrared spectrometer over the range 4000–250 cm^{-1} and at 4 cm^{-1} resolution. The spectrometer included a cesium-iodide beamsplitter and a deuterated triglycine-sulphate (DTGS) detector.

EXAFS spectra for the *K*-edges of Fe, Mn, and Ni were recorded in both transmission and fluorescence modes at room temperature on Station 8.1 at the CCLRC Daresbury synchrotron radiation source. The beam current at the CCLRC varied from 125 to 220 mA at an energy of 2 GeV. A Si(220) double-crystal monochromator was detuned 30–50% of the incident beam to minimize harmonic contamination. Data were calibrated by recording the spectra of the appropriate metal foils, using the values of 7112, 8333, and 6539 eV for the *K*-edges of iron, nickel, and manganese, respectively. The EXAFS data were collected in fluorescence mode using a solid-state, 13-element Canberra Ge detector. In the case of Ni, spectra were obtained in the fluorescence mode and an Al filter was used to reduce the Fe:Ni fluorescence signal ratio.

To obtain spectra of adequate quality, it was necessary to average several data sets for each sample used in the study. The number of spectra averaged for each sample varied between four to six. X-ray absorption spectra were first calibrated and then background subtracted and normalized by fitting polynomials to the pre-edge and post-edge regions. Curve fitting was performed in k-cubed (k^3) weighted data using the program EXCURV92 which utilizes single scattering curved-wave theory (Binsted *et al.*, 1992). The pro-

Table 2. Structural parameters for the cationic shells of hematite samples determined by EXAFS spectroscopy of the Fe, Ni, and Mn absorption edges.

Sample	R-factor	First O shell(s)			First cationic shell			Second cationic shell			Third cationic shell		
		CN[1]	R[2]	σ[3]	CN[1]	R[2]	σ[3]	CN[1]	R[2]	σ[3]	CN[1]	R[2]	σ[3]
Fe *K*-edge													
Natural hematite	24.5	2.9	1.93	.004	4.2	2.96	.009	2.9	3.38	.008	5.8	3.70	.016
		3.0	2.10	.012									
Hematite 4.6 mole % Al	28.4	2.8	1.95	.020	4.1	2.96	.020	3.3	3.35	.018	5.6	3.69	.018
		3.1	2.05	.021									
Hematite 15 mole % Al	24.1	2.8	1.93	.013	4.1	2.97	.019	3.2	3.36	.014	5.6	3.67	.026
		2.8	2.06	.011									
Hematite 3.3 mole % Mn	22.7	2.7	1.95	.009	4.2	2.96	.018	3.2	3.36	.015	5.7	3.69	.017
		2.7	2.07	.021									
Hematite 6.3 mole % Mn	28.7	2.6	1.96	.013	4.2	2.96	.017	3.1	3.38	.018	5.1	3.70	.016
		2.6	2.05	.016									
Hematite 1.1 mole % Ni	23.3	2.8	1.92	.014	4.0	2.95	.015	3.2	3.37	.014	4.8	3.70	.015
		2.7	2.07	.017									
Hematite 6.0 mole % Ni	31.4	3.0	1.92	.003	4.7	2.93	.015	2.7	3.38	.012	5.1	3.67	.015
		3.0	2.09	.008									
Ni *K*-edge													
Hematite 1.1 mole % Ni	46.1	3.0	1.97	.003	4.0	2.90	.014	3.0	3.41	.010	6.0	3.67	.012
		3.0	2.09	.001									
Hematite 6.0 mole % Ni	35.8	3.0	1.98	.004	4.0	2.92	.020	3.0	3.42	.017	6.0	3.66	.018
		3.0	2.10	.001									
Mn *K*-edge													
Hematite 3.3 mole % Mn	35.7	6.0	1.95	.022	4.0	2.94	.023	3.0	3.32	.004	6.0	3.70	.032
Hematite 6.3 mole % Mn	24.3	5.8	1.88	.012	3.5	2.66	.001	8.3	2.88	.009	5.1	4.04	.008

[1] CN = coordination number, estimated uncertainty ± 20%.
[2] R = shell radius, estimated uncertainty ± 0.03 Å.
[3] σ = Debye-Waller factor.
R-factor = residual from *least-squares*.

gram uses a non-linear *least squares* iteration. *Ab-initio* phase shifts and potentials were calculated using Von Barth ground state and the Hedin-Lundqvist exchange-correlation functional with a muffin-tin potential. The theoretical spectra were then calculated using the rapid curved-wave theory of Gurman *et al.* (1984). Theoretical spectra were generated by defining shells of backscatterers and then iterating the distances (R), Debye-Waller factors (σ), and coordination numbers (CN) to give the best agreement with experimental spectra.

A natural hematite sample (Off BM 1926, 518) from France, supplied by the Natural History Museum, London, was used as a reference material for the EXAFS analysis.

RESULTS AND DISCUSSION

Crystal properties

X-ray diffraction patterns for the samples showed all major peaks of hematite, except for the 15 mole % Al-substituted hematite, where peaks for this sample were fewer and very broad. Crystallographic properties derived from XRD data and surface-area values clearly show that increasing amounts of Al substitution in the hematite structure significantly decreased unit-cell dimensions (Table 1). The MCD along the two axes also decreased markedly for 15 mole % Al-substituted hematite compared to other samples, as did the specific surface area. There was a small increase in the *a* and *c* cell dimensions with increasing amounts of Mn and Ni substitution in hematite. This was associated with a decrease in the surface area of these samples (Table 1). Cornell *et al.* (1992) also observed an increase in the *a* cell dimension of hematite from 0.540 to 0.545 nm with 7 mole % Ni substitution in hematite. The increase in the cell dimension *a* can be attributed to the slightly larger radius of Ni^{2+} (0.070 nm) as compared to the Fe^{3+} ion (0.065 nm) which it replaces (Shannon and Prewitt, 1969).

No other crystalline phase was identified by XRD in any of the samples except for the hematite sample containing 6.3 mole % Mn, where a very small peak at ~0.71 nm was observed. This peak may be related to trace amounts of a phyllomanganate phase, which may have crystallized during the synthesis of hematite. Cornell and Giovanoli (1987) also observed a similar product during the synthesis of Fe oxides in the presence of 30 mole % Mn^{3+}.

EXAFS spectroscopy

Iron. According to the polyhedral concept, octahedra in hematite share one face [Fe-Fe distance, d(Fe-Fe) = 2.89 Å], three edges [d(Fe-Fe) = 2.97 Å], three double corners [d(Fe-Fe) = 3.37 Å], and six double

https://doi.org/10.1346/CCMN.2000.0480504 Published online by Cambridge University Press

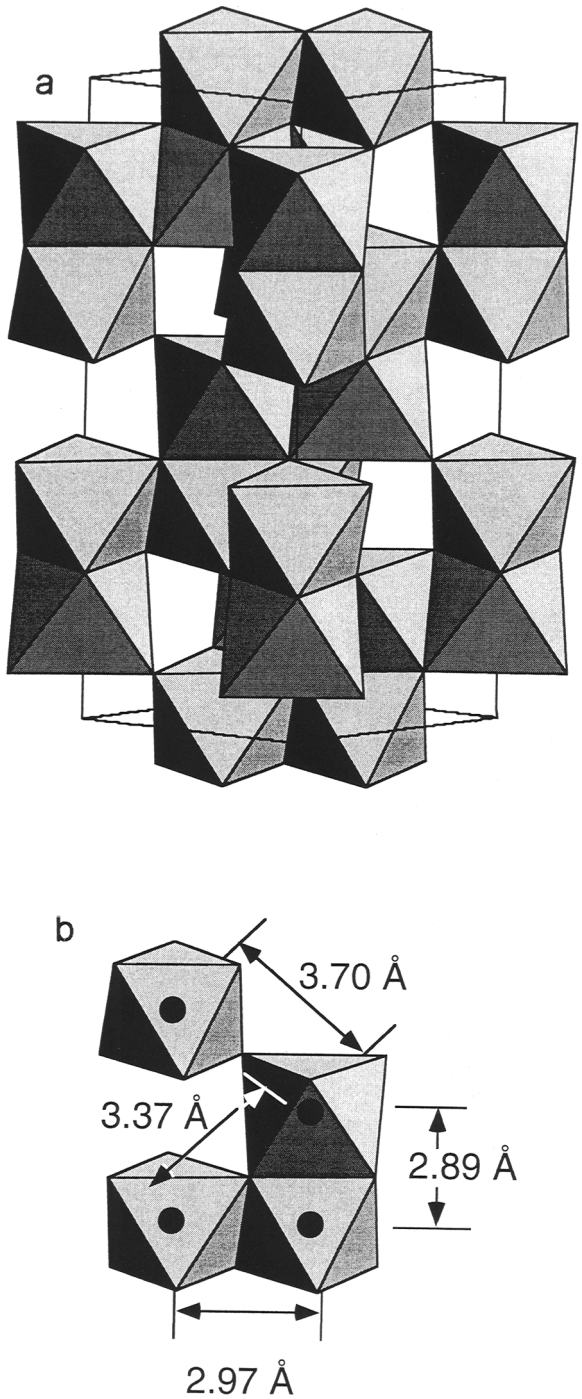

Figure 1. (a) Structural model of hematite. The unit cell is shown by the outline. (b) Face (2.89 Å), edge (2.97 Å), and double corner (3.37 and 3.70 Å) sharing of octahedra in hematite according to the polyhedral concept (Manceau and Combes, 1988).

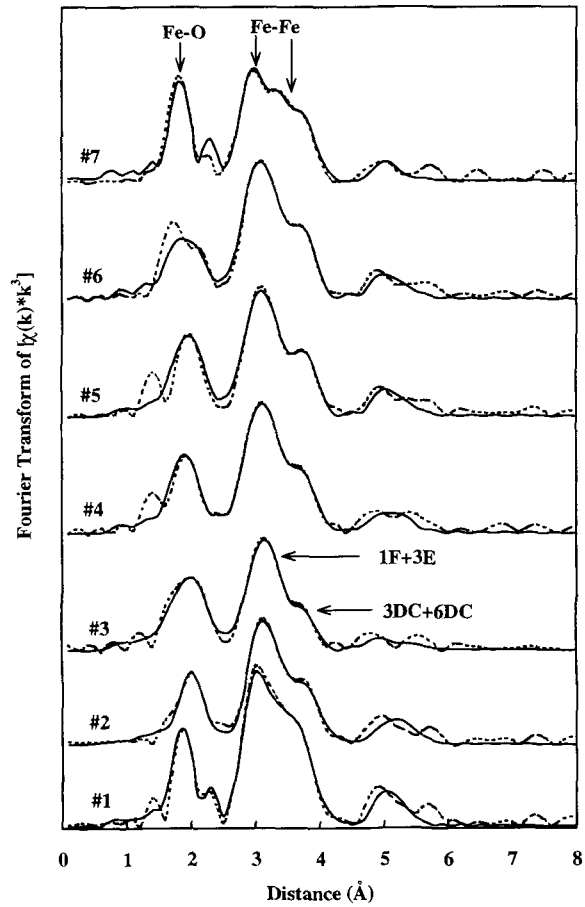

Figure 2. Fe *K*-edge Fourier transforms of natural (#1) and metal-substituted hematite samples: 4.6 mole % Al (#2), 15.0 mole % Al (#3), 3.3 mole % Mn (#4), 6.3 mole % Mn (#5), 1.1 mole % Ni (#6), and 6.0 mole % Ni (#7). The peaks corresponding to Fe-O and Fe-Fe shells (face 2.89 Å, edge 2.97 Å, and double corners 3.37 and 3.70 Å sharing of octahedra) are indicated by the arrows. Dotted lines are for experimental data and solid lines are for theoretical fits.

corners [d(Fe-Fe) = 3.70 Å] as shown in Figure 1 (Manceau and Combes, 1988). The Fe *K*-edge data for the Fe-Fe distances for the first three cationic shells agree very well with the ideal hematite structure (Figure 2; Table 2). The Fe-O distances for the first two oxygen shells for the octahedrally coordinated Fe also agree well with the ideal distances for the two oxygen shells (1.946 and 2.116 Å) in the hematite structure. Contribution to EXAFS of other O shells is very weak and their inclusion does not make any significant difference to Fe-Fe distances. The substitution of other cations, *i.e.,* Al, Mn, and Ni, does not seem to have any influence on the local structure around Fe atoms in the structure of hematite.

Despite similarities in the local environment around the Fe atom, various samples yielded different Fourier transforms (FTs) of Fe *K,* as shown in Figure 2. The

https://doi.org/10.1346/CCMN.2000.0480504 Published online by Cambridge University Press

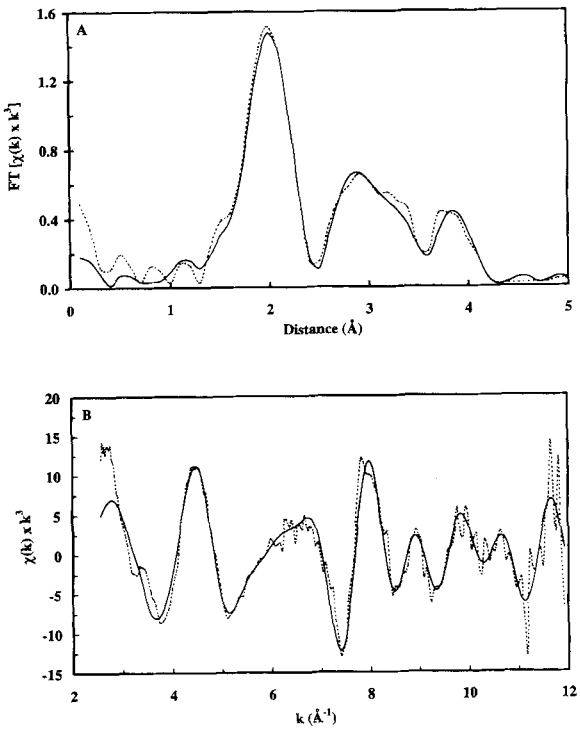

Figure 3. The EXAFS data for the Ni *K*-edge of 6 mole % Ni-substituted hematite. (a) Fourier-transform (FT) and (b) k^3-weighted EXAFS oscillations [$\chi(k)$] analyzed in k-space, where k is the momentum of the photoelectron in $Å^{-1}$. Dotted lines are for the experimental data and solid lines for the simulated data. Parameters obtained from the fit are given in Table 2.

first cationic peak on the FT corresponds to the unresolved shortest shells for Fe at 2.89 and 2.97 Å and has the highest intensity in all the samples. The second cationic peak fits to yet another two unresolved shells at 3.37 and 3.70 Å, and the intensity of this peak is at a maximum for natural hematite. The FT of 6 mole % Ni-substituted hematite shows three distinct peaks for cationic shells between 3–4 Å, but the best fit for the spectrum is obtained with two shells at a distance of 3.38 and 3.67 Å. The peak at ~5 Å, which is related to another Fe-Fe shell, has the weakest intensity in 15 mole % Al-substituted hematite amongst all of the samples studied, and this is consistent with structural disorder in the sample as indicated by XRD.

Nickel. Hematites substituted with 1.1 and 6.0 mole % Ni show nearest neighbor and short-range structure identical to that of Fe in hematite, and this implies that Ni^{2+} is substituting for Fe^{3+} (Figure 3; Table 2). Moreover, the Ni-O bond length is similar to that of the Fe-O bond length, which is consistent with the ionic radii of Ni^{2+} and Fe^{3+} being similar (Shannon and Prewitt, 1969). Presumably, the uptake of Ni^{2+} is accompanied by a coupled substitution involving H^+ or vacancies in

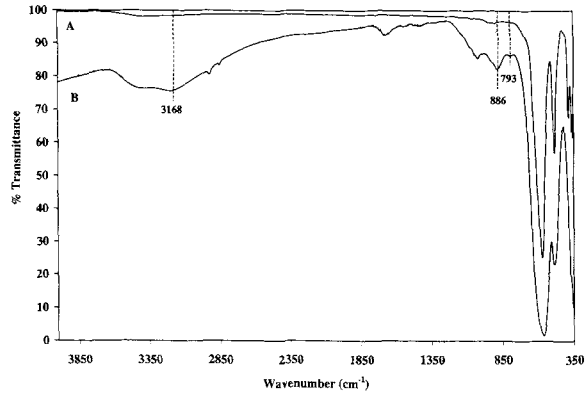

Figure 4. IR spectra of (A) pure hematite and (B) 15 mole % Ni-substituted hematite sample. The Ni-substituted sample shows an OH stretch band at 3168 cm^{-1} and Fe-OH bending modes at 892 and 796 cm^{-1}. These bands are analogous to the OH bands in goethite.

the octahedral cation sites, which cannot be determined by EXAFS.

Infrared spectroscopy of 15 mole % Ni-substituted hematite exhibits bands at 3168, 886, and 793 cm^{-1} which are analogous to OH bands at 3168, 892, and

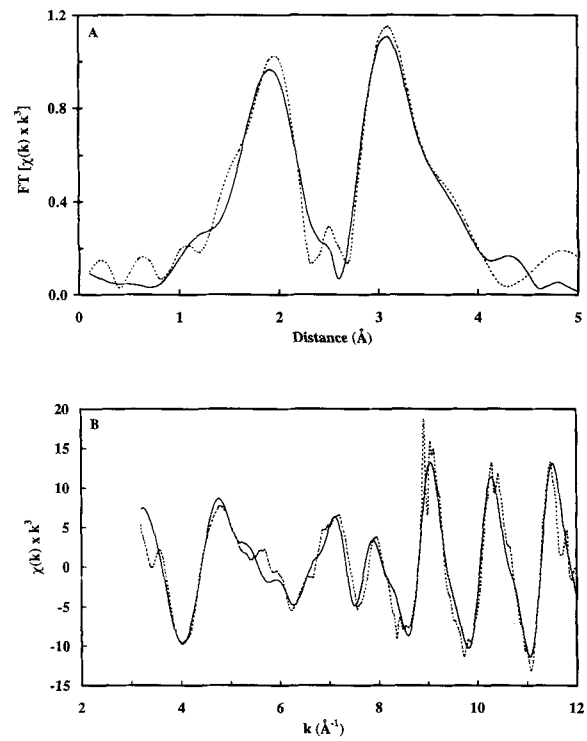

Figure 5. The EXAFS data for the Mn *K*-edge of 3.3 mole % Mn-substituted hematite. (a) Fourier-transform (FT) and (b) k^3-weighted EXAFS oscillations [$\chi(k)$] analyzed in k-space, where k is the momentum of the photoelectron in $Å^{-1}$. Dotted lines are for the experimental data and solid lines for the simulated data. Parameters obtained from the fit are given in Table 2.

https://doi.org/10.1346/CCMN.2000.0480504 Published online by Cambridge University Press

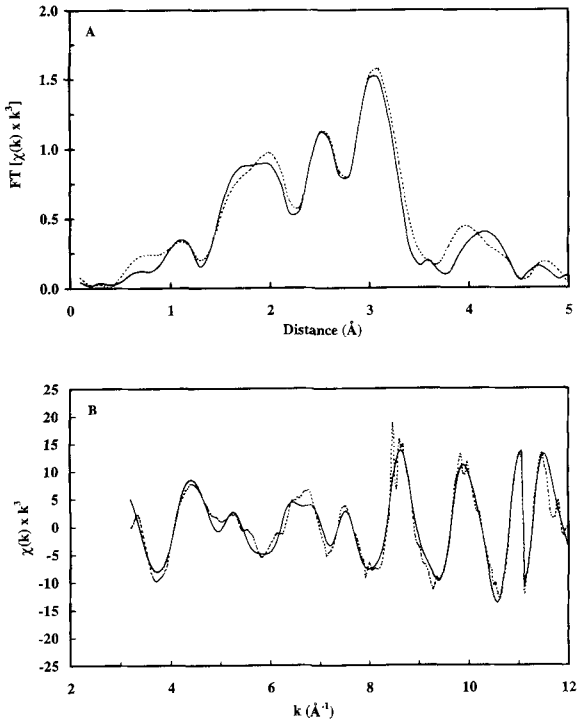

Figure 6. The EXAFS data for the Mn *K*-edge of 6.3 mole % Mn-substituted hematite. (a) Fourier-transform (FT) and (b) k^3-weighted EXAFS oscillations [χ(k)] analyzed in k-space, where k is the momentum of the photoelectron in $Å^{-1}$. Dotted lines are for the experimental data and solid lines for the simulated data. Parameters obtained from the fit are given in Table 2.

796 cm^{-1} in goethite (Figure 4). These bands were absent in the IR spectrum of the pure hematite sample (Figure 4A). The result is consistent with the presence of structural OH^- to compensate for Ni^{2+} replacing Fe^{3+} but it is noted that such an OH^- substitution also occurs in non-substituted hematite synthesized at low temperatures (Stanjek and Schwertmann, 1992). These results indicate that with Ni^{2-} substitution for Fe^{3-} there is a corresponding substitution of OH^- for O^{2-} in the hematite structure.

Manganese. The ionic radii of Mn^{3+} (0.645 nm) and Fe^{3+} (0.65 nm) are nearly identical, but Mn^{3-} has one less electron in the 3*d* orbital than Fe^{3-}. The d^4 electron configuration of Mn^{3-} undergoes a large static Jahn-Teller distortion in octahedral coordination (Burns, 1970). This may limit the substitution of Mn in hematite. For 3.3 mole % Mn-substituted hematite, a reasonable hematite-like short-range structure is found but with a large (0.022) Debye-Waller factor for the first coordination shell (Table 2; Figure 5). The large Debye-Waller factor may reflect the strong vibronic coupling associated with the d^4 electronic configuration. This is the same vibronic coupling which yields the Jahn-Teller distortion of the Mn^{3-} coordination site; however, in hematite, no distortion of the coordination shell is resolved in the fit.

The sample with 6.3 mole % Mn shows a short-range structure that is very different from that of ideal hematite. The spectrum fits reasonably well to the ramsdellite (MnO_2) structure (Figure 6; Table 2) showing Mn shells at 2.66 and 2.88 Å. In ramsdellite, the distances for the first three cationic shells are at 2.659, 2.848, and 3.582 Å. The third cationic shell in 6.3 mole % Mn-substituted hematite at a distance of 4.09 Å did not fit to the structure of ramsdellite, which may be related to the presence of a mixture of Mn phases. The results show that Mn in the 6.3 mole % sample is not substituting for Fe in the hematite structure. Earlier work on Mn substitution in hematite indicated that ≤5 mole % Mn can be incorporated in the hematite structure and any additional Mn is either adsorbed or precipitated as a separate phase (Cornell and Giovanoli, 1987; Cornell *et al.*, 1990).

We tentatively propose that other cations showing a strong Jahn-Teller effect will have a limited solubility in Fe_2O_3. In particular, Cu^{2+} should be much less soluble in Fe_2O_3 than other metals of comparable charge and ionic radius.

CONCLUSIONS

EXAFS spectroscopy showed that hematites synthesized by coprecipitation from an Fe-metal nitrate solution at alkaline pH can be substituted by ≤6 mole % Ni^{2+} for Fe^{3+} in the structure. The substitution of Ni^{2+} for Fe^{3-} in the hematite structure is accompanied by a corresponding substitution of OH^- for O^{2-} as indicated by IR spectroscopy. For Mn^{3+}, the substitution of Mn^{3+} for Fe^{3+} exists only to ≤3.3 mole %. For larger amounts of Mn, a separate phase (ramsdellite) is formed. The local environment around Fe^{3+} atoms remains similar for a range of substitution of Al^{3+}, Mn^{3-}, and Ni^{2+} in the hematite structure.

ACKNOWLEDGMENTS

The authors wish to thank the EPSRC for the financial support and for the provision of beamtime (27/229) at the CCLRC Daresbury. We are grateful to J. Cook and A. Apsley for their help in the collection of EXAFS data and T. Fraser for the IR spectroscopy. We also thank S. Guggenheim, A. Scheinost, and an anonymous referee for their critical review and helpful suggestions.

REFERENCES

Bigham, J.M., Golden, D.C., Bowen, L.H., Buol, S.W., and Weed, S.B. (1978) Iron oxide mineralogy of well-drained Ultisols and Oxisols. I. Characterization of iron oxides in soil clays by Mössbauer spectroscopy, X-ray diffractometry, and selected chemical techniques. *Soil Science Society of America Journal*, **42**, 816–825.

Binsted, N., Campbell, J.W., Gurman, S.J., and Stephenson, P.C. (1992) EXCURV92 Program. CCLRC, Daresbury Laboratory Program, Warrington, UK.

Burns, R.G. (1970) *Mineralogical Applications of Crystal Field Theory.* Cambridge University Press, Cambridge, 224 pp.

Combes, J.M., Manceau, A., and Calas, G. (1990) Formation of ferric oxides from aqueous solutions: A polyhedral approach by X-ray absorption spectroscopy: II. Hematite formation from ferric gels. *Geochimica et Cosmochimica Acta,* **54,** 1083–1091.

Cornell, R.M. and Giovanoli, R. (1987) Effect of manganese on the transformation of ferrihydrite into goethite and jacobsite in alkaline media. *Clays and Clay Minerals,* **35,** 11–20.

Cornell, R.M., Giovanoli, R., and Schneider, W. (1990) Effect of cysteine and manganese on the crystallization of noncrystalline iron(III) hydroxide at pH 8. *Clays and Clay Minerals,* **38,** 21–28.

Cornell, R.M., Giovanoli, R., and Schneider, W. (1992) The effect of nickel on the conversion of amorphous iron(III) hydroxide into more crystalline iron oxides in alkaline media. *Journal of Chemical Technology and Biotechnology,* **53,** 73–79.

Fischer, W.R. and Schwertmann, U. (1975) The formation of hematite from amorphous iron(III)-hydroxide. *Clays and Clay Minerals,* **23,** 33–37.

Gurman, S.J., Binsted, N., and Ross, I. (1984) A rapid, exact curved-wave theory for EXAFS calculations. *Journal of Physics. C,* **17,** 143–151.

Klug, H.P. and Alexander, L.E. (1974) *X-ray Diffraction Procedures for Polycrystalline and Amorphous Materials, 2nd edition,* John Wiley and Sons, New York, 966 pp.

Kosmas, C.S., Franzmeier, D.P., and Schulz, D.G. (1986) Relationship among derivative spectroscopy, color, crystallite dimensions and Al-substitution of synthetic goethites and hematites. *Clays and Clay Minerals,* **34,** 625–634.

Manceau, A. and Combes, J.M. (1988) Structure of Mn and Fe oxides and oxyhydroxides: A topological approach by EXFAS. *Physics and Chemistry of Minerals,* **15,** 283–295.

McKeague, J.A. and Day, J.H. (1966) Dithionite- and oxalate-extractable Fe and Al as aids in differentiating various classes of soils. *Canadian Journal of Soil Science,* **46,** 13–22.

Novak, G.A. and Colville, A.A. (1989) A practical interactive least-squares cell-parameter program using an electronic spreadsheet and a personal computer. *American Mineralogist,* **74,** 488–490.

Parfitt, R.L. (1989) Optimum conditions for extraction of Al, Fe and Si from soils with acid oxalate. *Communications in Soil Science Plant Analysis,* **20,** 801–816.

Schwertmann, U., and Taylor, R.M. (1989) Iron Oxides. In *Minerals in Soil Environments,* J.B. Dixon and S.B. Weed, eds., Soil Science Society of America, Madison, Wisconsin, USA, 379–438.

Schwertmann, U., Fitzpatrick, R., Taylor, R.M., and Lewis, D.G. (1979) The influence of aluminum on iron oxides. Part II. Preparation and properties of Al-substituted hematites. *Clays and Clay Minerals,* **27,** 105–112.

Shannon, R.D. and Prewitt, C.T. (1969) Effective ionic radii in oxides and fluorides. *Acta Crystallographica,* **B25,** 925–946.

Sidhu, P.S., Gilkes, R.J., and Posner, A.M. (1980) The behavior of Co, Ni, Zn, Cu, Mn and Cr in magnetite during alteration to maghemite and hematite. *Soil Science Society of America Journal,* **44,** 135–138.

Singh, B. and Gilkes, R.J. (1992) Properties and distribution of iron oxides and their association with minor elements in the soils of south-western Australia. *Journal of Soil Science,* **43,** 77–98.

Stanjek, H. and Schwertmann, U. (1992) The influence of aluminum on iron oxides. Part XVI: Hydroxyl and aluminum substitution in synthetic hematites. *Clays and Clay Minerals,* **40,** 347–354.

Trolard, F., Bourrie, G., Jeanroy, E., Herbillon, A.J., and Martin, H. (1995) Trace metals in natural iron oxides from laterites: A study using selective kinetic extraction. *Geochimica et Cosmochimica Acta,* **59,** 1285–1297.

Vandenberghe, R.E., Verbeeck, A.E., DeGrave, E., and Steir, W. (1986) ^{57}Fe Mössbauer effect study of Mn-substituted goethite and hematite. *Hyperfine Intercations,* **29,** 1157–1160.

E-mail of corresponding author: b.singh@acss.usyd.edu.au

(Received 20 July 1999; accepted 26 April 2000; Ms. 364; A.E. William F. Bleam)